CIRP Journal of Manufacturing Science and Technology 30 (2020) 131–139

Contents lists available at ScienceDirect

CIRP Journal of Manufacturing Science and Technology

journal homepage: www.elsevier.com/locate/cirpj

Mechanics of milling 48-2-2 gamma titanium aluminide

Abbas Hussain[a], S. Ehsan Layegh[c], Ismail Lazoglu[a,*], Pedro-J. Arrazola[b], Xabier Lazcano[b], Patxi-X. Aristimuño[b], Omer Subasi[a], I. Enes Yigit[a], Çağlar Öztürk[a], Çağlar Yavaş[d]

[a] Koc University, Manufacturing and Automation Research Center, Istanbul 34450, Turkey
[b] Mondragon University, Faculty of Engineering, Mondragon 20500, Spain
[c] MEF University, Istanbul 34396, Turkey
[d] Karcan Cutting Tools, Eskisehir 26110, Turkey

ARTICLE INFO

Article history:
Available online 23 June 2020

Keywords:
Milling
Gamma titanium aluminide
Coating

ABSTRACT

Accurate and fast prediction of cutting forces is important in high-performance cutting in the aerospace industry. Gamma titanium aluminide (γ-TiAl) is a material of choice for aerospace and automotive applications due to its superior thermo-mechanical properties. Nevertheless, it is a difficult to machine material. This article presents the prediction of cutting forces for Ti-48Al-2Cr-2Nb (48-2-2) γ-TiAl in milling process using orthogonal to oblique transformation technique. The novelty of this paper lies in reporting the orthogonal database of 48-2-2 γ-TiAl. Fundamental cutting parameters such as shear stress, friction angle and shear angle are calculated based on experimental measurements. Friction coefficients are identified for two different coating conditions which are AlTiN, and AlCrN on carbide tools. Predicted results are validated with the experimental cutting forces during end milling and ball-end milling operations for different cutting conditions. The simulated results showed good agreement with the experimental results, which confirms the validity of the force model.

Introduction

The use of advanced lightweight structural materials is a key point for aerospace and automotive applications to improve engine performances and efficiency, as well as to satisfy the increasingly restrictive environmental regulations, aimed at reaching a decisive lessening of CO_2 emissions [1]. In this context, intermetallic aero-engine materials, such as γ-TiAl, have been identified as strategically critical materials to be used in both non-rotating and rotating components, e.g. blade manufacturing. They provide a remarkable strength-to-weight ratio, approximately half the density of nickel-based superalloys, high stiffness, high elastic modulus, strength retention at elevated temperatures, oxidation resistance, and good creep properties [2,3].

However, the attractive mechanical and thermal properties, become a drawback when dealing with machining, as it occurs with many other materials. As it has been shown in several conventional machining publications, machinability of γ-TiAl is poor because of its low ductility combined with high hardness and brittleness at room temperature, low thermal expansion, low fracture toughness and chemical reactivity with many tool materials [4,5]. In consequence, the machining cost is high, which can restrict the widespread use of these materials in the industry.

Several research studies have been carried out in the last years dealing with the machinability properties of γ-TiAl. Mantle et al. [6] investigated the surface integrity of γ-TiAl, Ti–45Al–2Nb–2Mn-0.8 vol.% TiB_2XD by performing high-speed milling operations. Experiments were carried out using coated tungsten carbide ball-end mill in up milling and down milling directions. Priarone et al. [7] studied the effect of cutting tool angles and cutting-edge preparation in machinability of Ti-48Al-2Cr-2Nb EBM sintered γ-TiAl. All the milling operations were performed in down milling mode with coated and uncoated carbide end mills. Beranoagirre et al. [8] provided the specific cutting force coefficients obtained from the mechanistic calibration method for three different types of γ-TiAl alloys: the MoCuSi type in ingot and extruded form, and the TNB type in ingot form. They performed milling experiments and studied the tool wear for different cutting conditions and found that the cutting velocity is the determining factor in tool life. Settineri et al. [9] performed turning and milling experiments on three different γ-TiAl alloys: Ti–48Al–2Cr–2Nb, Ti–43.5Al–4Nb–1Mo–0.1B, and Ti–45Al–2Nb–2 Mn-0.8 vol.% TiB_2 XD, focusing on machinability and material characterization. The experimental results were extremely dissimilar due to the different alloying elements which affected the mechanical and thermal material properties. Hood et al. [10] investigated the surface integrity by

* Corresponding author.
E-mail address: ilazoglu@ku.edu.tr (I. Lazoglu).

https://doi.org/10.1016/j.cirpj.2020.05.001
1755-5817/

performing slot milling on Ti–45Al–2Nb–2Mn-0.8 vol.%, TiB_2 using AlTiN coated WC ball nose end mills.

Although machining of γ-TiAl alloys has been previously researched in the literature, no studies have been carried out to develop an orthogonal cutting database for the prediction of cutting forces for γ-TiAl in oblique and 3D processes such as flat and ball-end milling. The creation of such a database is crucial for accurate and fast predictions of cutting forces employed in high-performance machining of aeronautic components such as blades. This implies that industrial parameters such as surface roughness, the possibility of chatter or dimensional tolerances can be accurately predicted.

A fundamental cutting parameter database independent of cutter geometry is required to calculate the cutting forces in a machining operation. This database is then used to calculate the specific cutting coefficients by applying an analytical orthogonal to oblique transformation model [11]. In addition, this model allows the prediction of cutting forces of complex operations such as ball-end milling [12]. This approach can also be implemented to investigate the effects of cutting parameters on machining performance [13].

High-performance coatings have become a successful standard for increasing the efficiency of machining tools in the industry over the last decade [14,15]. The current study focuses on establishing an orthogonal cutting database for 48-2-2 γ-TiAl for different tool coatings; AlTiN and AlCrN coatings. For cutting force predictions, an analytical force model and the orthogonal to oblique transformation method is employed. The model is then validated for end milling and ball-end milling operations for different cutting conditions, demonstrating good agreement between experimental and modeled results.

Mechanics of milling operation

Milling operation is one of the most fundamental metal cutting operations that is extensively used in the manufacturing of complex components in high-tech fields such as aerospace, automotive and biomedical industries. Unlike turning, which is a continuous cutting operation, milling is an interrupted machining operation. During milling operation, the cutting edges repeatedly enter and exit the engagement domain. Therefore, the cutting forces are harmonic and the simulation of cutting forces is more complicated. The geometry of the milling tool and the mechanics of the process are illustrated in Fig. 1(a).

Elemental cutting forces in end milling operation can be analytically modeled using Eq. (1). In this set of equations dF_t,dF_r and dF_a are the differential cutting forces in tangential, radial and axial directions, respectively. Moreover, $h(\phi)$ and dz denote the uncut chip thickness and elemental length of the cutting edge in the axial direction. $K_{tc}, K_{rc}, K_{ac}, K_{te}, K_{re}$ and K_{ae} are the specific cutting and edge coefficients that are associated with the cutting and ploughing phenomena in the metal cutting process:

$$\left.\begin{aligned} dF_t &= [K_{tc}h(\phi) + K_{te}]dz, \\ dF_r &= [K_{rc}h(\phi) + K_{te}]dz, \\ dF_a &= [K_{ac}h(\phi) + K_{ae}]dz, \end{aligned}\right\} \quad (1)$$

The accuracy of the analytical model is highly dependent upon the accurate prediction of the cutting force coefficients and edge coefficients. Different approaches have been suggested in the literature to predict the cutting coefficients [16–20]. The advantage of using orthogonal to oblique transformation technique over other methods is that the cutting coefficients can be predicted before the manufacturing of the tool. This method is independent of cutter geometry and can be used to simulate the cutting forces for any metal cutting process alike. Orthogonal to oblique transformation technique is based on the measurement of chip thicknesses and the cutting forces in the tangential and feed directions in an orthogonal turning test. The measurements are used to calculate the fundamental cutting parameters, including shear stress, shear angle and friction angle. Transformation of these parameters are then utilized to model oblique cutting processes such as the milling operation. In this paper, using the orthogonal cutting forces, the cutting force coefficients and edge coefficients in Eq. (1) are estimated [21]. The geometry of the orthogonal cutting is illustrated in Fig. 1(b). The fundamental parameters for orthogonal to oblique transformation can be predicted from Eqs. (2)–(6):

$$\beta_a = \alpha_r + \tan^{-1}\frac{F_{fc}}{F_{tc}} \quad (2)$$

$$\mu = \tan(\beta_a) \quad (3)$$

$$\phi_c = \frac{\pi}{4} = \frac{(\beta_a - \alpha_r)}{2} \quad (4)$$

$$\tau_s = \frac{F\cos(\phi_c + \beta_a - \alpha_r)\sin\phi_c}{bh} \quad (5)$$

$$r_c = \frac{\tan(\phi_c)}{\cos(\alpha_r)(\tan(\alpha_r)\tan(\phi_c) + 1)} \quad (6)$$

where $\beta_a, \alpha_r, F_{fc}, F_{tc}, \mu, \phi_c, \tau_s, F, b, h$ and r_c are friction angle, rake angle, average feed cutting force, average tangential cutting force, the coefficient of friction, shear angle, shear stress, average

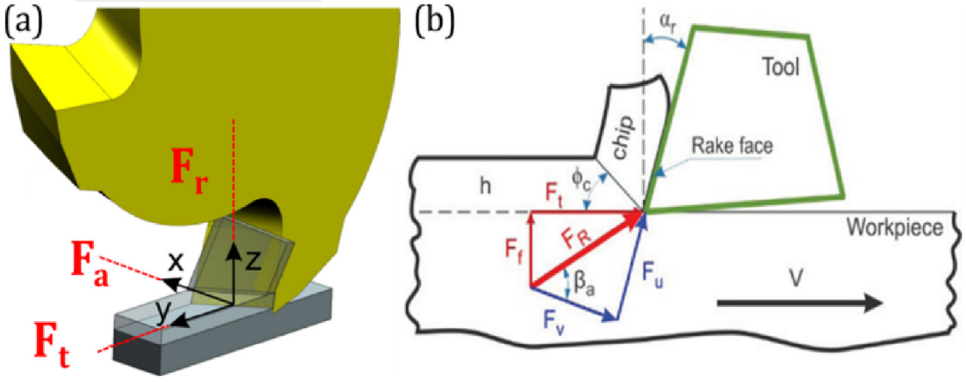

Fig. 1. Geometry of (a) milling, and (b) orthogonal turning operation.

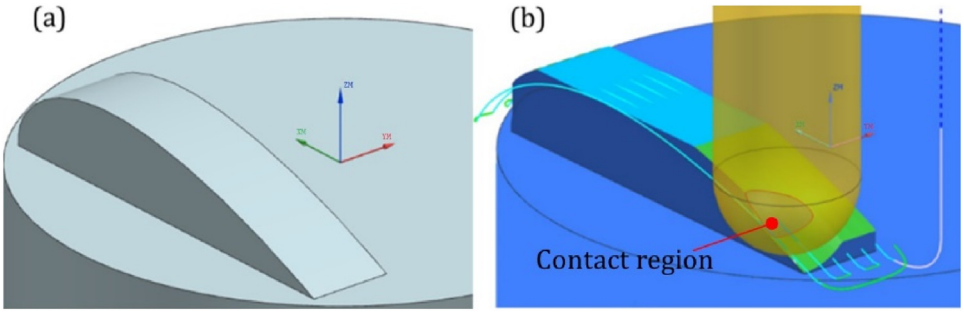

Fig. 2. (a) CAD model of the freeform surface; (b) CAM simulation and tool-workpiece contact region.

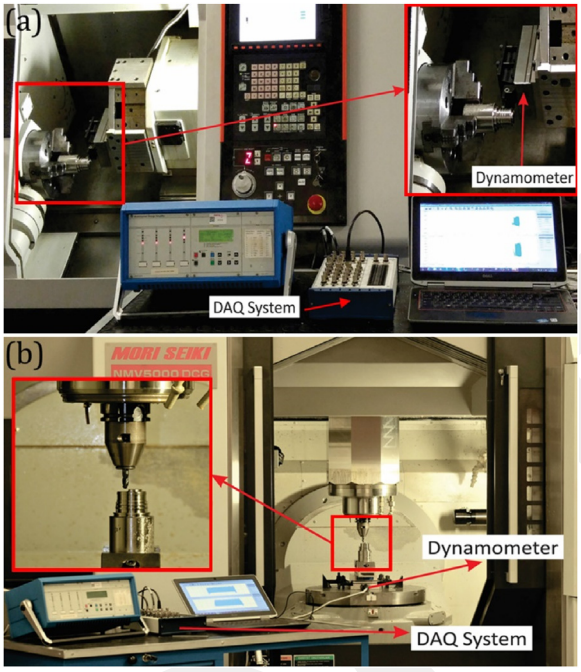

Fig. 3. (a) Orthogonal turning setup and (b) milling test setup and for 48-2-2 γ-TiAl machining (DAQ: data acquisition).

resultant force, the width of cut, uncut chip thickness, and chip thickness ratio in orthogonal turning, respectively. Due to the low machinability of γ-TiAl, the produced chips during the machining process are expected to be discontinuous, making the deformed chip thickness measurement and empirical calculation of chip ratio challenging. To tackle this problem, the minimum energy principle is employed to estimate the shear angle as given in Eq. (4). This model assumes that the shear stress on the shear plane is equivalent to the yield shear stress of the material and that the shear plane is thin [22].

Cutter-workpiece engagement model for ball-end milling

The ball-end milling process is widely used in the machining of free form surfaces especially in the automobile, aerospace, and die and mold industries. Owing to the geometry of the ball-end milling tool, the engagement area does not remain constant and the complete cutting-edge length is not in contact with the workpiece during the freeform surface machining. In this study, the cutting forces for freeform ball-end milling are predicted by employing a solid modeler-based engagement model to predict the contact region between the tool and the workpiece. First, the contact surface between the tool and the workpiece is calculated at each cutter location, then the swept volume of the cutting tool is calculated from the cutter location (CL) file. The entrance and exit angles of each discrete cutting disk are calculated after subtracting the swept volume from a blank workpiece. These angles are used as an input for the force model. A detailed explanation of the employed engagement model is provided in [23]. A sample contact region for a given cutter location on a freeform milling surface is shown in Fig. 2.

Experimental setup

The experimental stage of this work consisted of both orthogonal turning and milling of 48-2-2 γ-TiAl, a difficult to cut material. The obtained as-cast workpiece specimen is reported

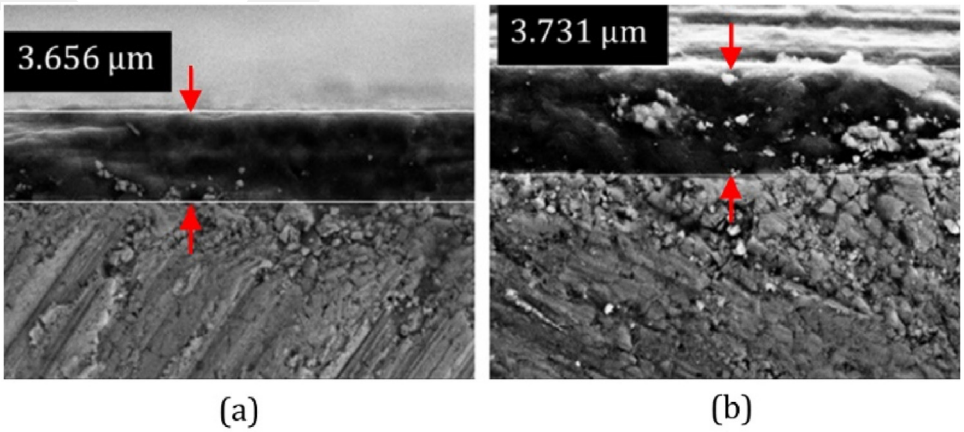

Fig. 4. Flat end mill coating thicknesses for (a) AlCrN coating, and (b) AlTiN coating.

to have 24 ± 2 HRC with 326 MPa yield strength, 422 MPa ultimate tensile strength and %1.7 elastic strain at 23°, and 384 MPa yield strength, 474 MPa ultimate tensile strength and 5.1% elastic strain at 650° [26,27]. Orthogonal turning tests were performed to establish the orthogonal database, whereas the milling tests were conducted to validate the predicted cutting forces obtained from the developed database.

Orthogonal turning setup

Orthogonal cutting tests were performed on a Mazak Quick Turn Nexus 150 turning center as shown in Fig. 3(a). A grooved 48-2-2 γ-TiAl workpiece with 55 mm diameter and 2 mm width of cut was used during tests. The inclination angle was set to zero degrees to have an orthogonal cutting condition. All experimental tests were performed for 40 m/min cutting velocity and 0.06, 0.08 and 0.100 mm/rev feedrates. Cutting operations were conducted with a 4° rake angle and tungsten carbide inserts with two different coatings: AlCrN and AlTiN coatings. With scanning electron microscope measurements, the edge radii of the turning inserts were identified as 15 μm for the AlCrN coated tool and 16 μm for the AlTiN coated tool. No coolant was used during the machining and cutting forces were measured using Kistler 9257B table type dynamometer.

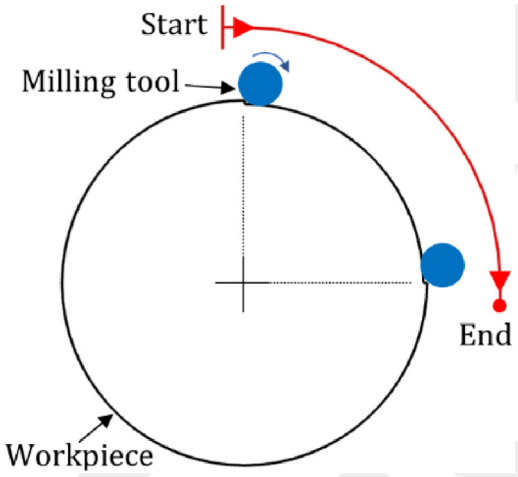

Fig. 5. Toolpath for flat end milling.

Milling setup

A set of experimental tests consisting of flat and ball-end milling were performed on a 5-axis Mori Seiki NMV5000 DCG machining center as shown in Fig. 3(b). Once again, all the milling tests were conducted at dry conditions and a Kistler 9257B table type dynamometer was utilized for cutting force data collection.

Flat end milling tests were conducted with a 36.5° helix angle, 8° rake angle, 12 mm diameter, four fluted tungsten carbide end mills having two different coating conditions: AlCrN and AlTiN coating. The thicknesses of the coatings were measured using a scanning electron microscope (SEM) shown in Fig. 4. Cutting force data was acquired during down milling operation for the tool path shown in Fig. 5. The cutting conditions are tabulated in Table 1.

The estimated cutting forces for ball-end milling were validated by performing down end milling and freeform surface milling using AlCrN coated, four fluted, tungsten carbide ball-end mill with 30° nominal helix angle, 8 mm nominal diameter, and 5° rake angle. The cutting conditions are tabulated in Tables 2 and 3. The cutting tools used in the study are shown in Fig. 6

Table 1
Flat end milling cutting conditions for 48-2-2 γ-TiAl.

Cutting velocity [m/min]	Depth of cut [mm]	Width of cut [mm]	Feedrate [mm/tooth]
15	2	0.5	0.04, 0.05, 0.07, 0.08

Table 2
Ball-end milling cutting conditions for 48-2-2 γ-TiAl in down end milling.

Cutting velocity [m/min]	Depth of cut [mm]	Width of cut [mm]	Feedrate [mm/tooth]
48	3	0.5	0.04, 0.06, 0.08

Table 3
Ball-end milling cutting conditions for 48-2-2 γ-TiAl in freeform milling.

Cutting velocity [m/min]	Stepover [mm]	Feedrate [mm/tooth]
40	1	0.06

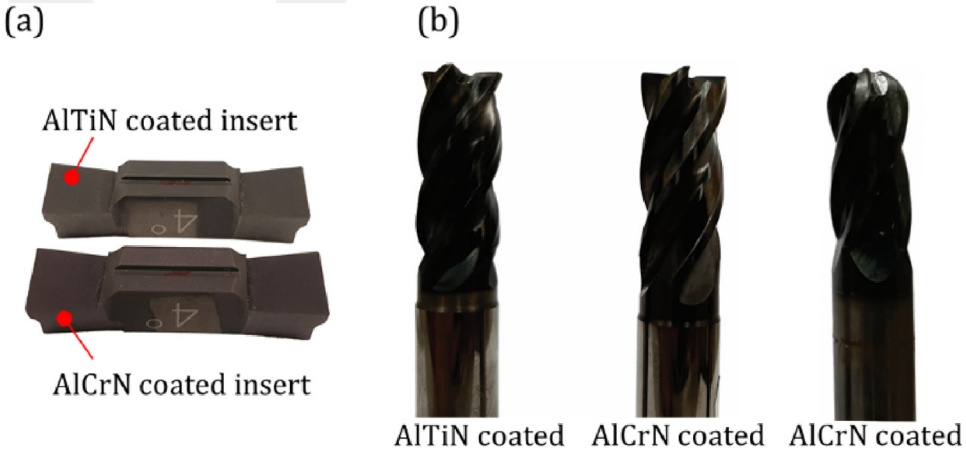

Fig. 6. Cutting tools used in the study; (a) coated turning inserts, (b) coated end mills and ball-end mill.

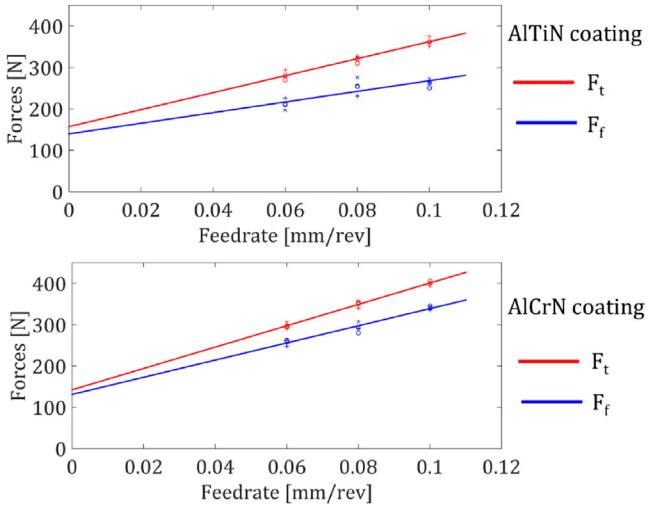

Fig. 7. Cutting forces measured during orthogonal turning of 48-2-2 γ-TiAl for 4° rake angle and different coatings.

Results and discussion

Orthogonal cutting of 48-2-2 γ-TiAl

The measured tangential and feed forces from orthogonal turning for different feedrates are shown in Fig. 7. These cutting forces were used to calculate the fundamental cutting parameters such as shear stress, shear angle, friction angle and chip ratio. The calculated orthogonal cutting parameters for different coatings are tabulated in Table 4 for the 4° rake angle insert. Results showed that the AlCrN coating has a smaller shear angle as compared to the AlTiN coating. In the cutting process, the chip thickness, shear angle and shear plane are interrelated to each other. A smaller shear angle is associated with a longer shear plane and a relatively large chip thickness. On the other hand, a large shear angle indicates a small shear plane and during the cutting process, produced chips are relatively thinner [24]. These result in less force needed to shear off the chips, implying that a lower friction coefficient dictates the process.

Table 4
Orthogonal to oblique database for 48-2-2 γ-TiAl.

Parameters	AlTiN	AlCrN
Chip ratio (r_c)	0.54 ± 0.01	0.46 ± 0.01
Friction angle (β_a)	$35.6° \pm 0.9$	$42.6° \pm 0.8$
Friction coefficient (μ)	0.72 ± 0.02	0.92 ± 0.02
Shear angle (ϕ_c)	$29.2° \pm 0.3$	$25.7° \pm 0.2$
Shear stress (τ_s)	289.1 ± 14.2 MPa	311.5 ± 6.7 MPa
K_{te}	78	71
K_{re}	70	66

The friction coefficient plays an important role in the tool life and workpiece integrity [25]. The friction coefficient identified from the orthogonal turning showed that the AlCrN coating had the highest friction coefficient as compared to the AlTiN coating. No significant change in shear stress is observed by changing the coatings.

Flat end milling of 48-2-2 γ-TiAl

The cutting coefficients for milling operation were determined from orthogonal to oblique transformation technique, and employing the analytical model shown in Eq. (1) the cutting forces were simulated. The calculated edge cutting coefficients from orthogonal force data are shown in Table 4. The estimated and measured cutting forces component for flat end milling for different coatings and feedrates are compared in Figs. 8 and 9. It can be inferred from Fig. 8 that the suggested force model is able to predict the cutting forces within a 20% error band for AlTiN coated tools. However, while the recorded tangential forces were found to be in close agreement with the force estimation model for the AlCrN coated tool, there is a mismatch for the radial force comparison. This sub-

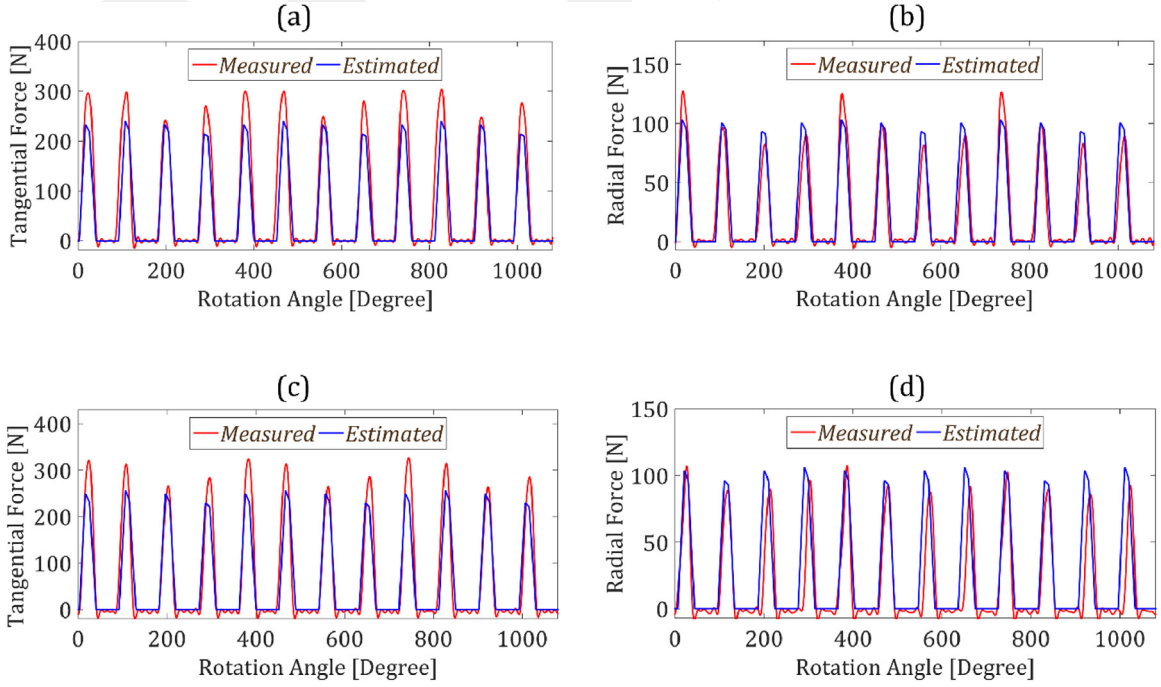

Fig. 8. Measured and estimated cutting forces for the AlTiN coated tool for flat end down-milling: Cutting forces in (a) tangential and (b) radial directions with a feedrate of 64 mm/min; cutting forces in (c) tangential and (d) radial directions with a feedrate of 88 mm/min.

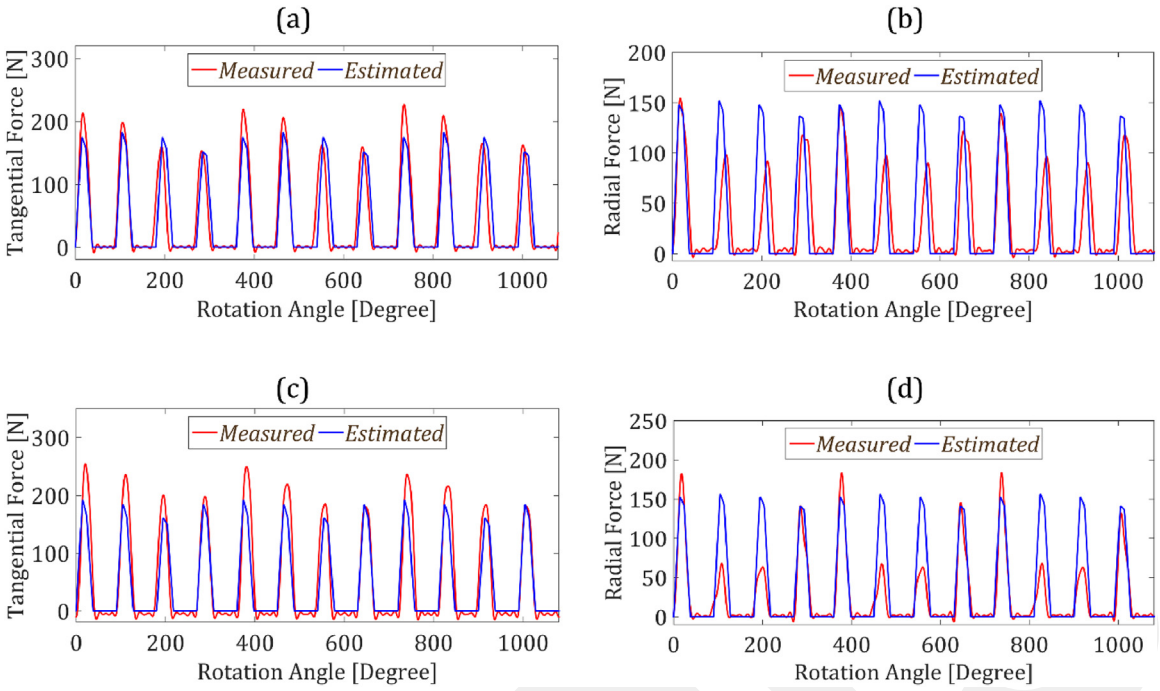

Fig. 9. Measured and estimated cutting forces for the AlCrN coated tool for flat end down-milling: Cutting forces in (a) tangential and (b) radial directions with a feedrate of 64 mm/min; cutting forces in (c) tangential and (d) radial directions with a feedrate of 88 mm/min.

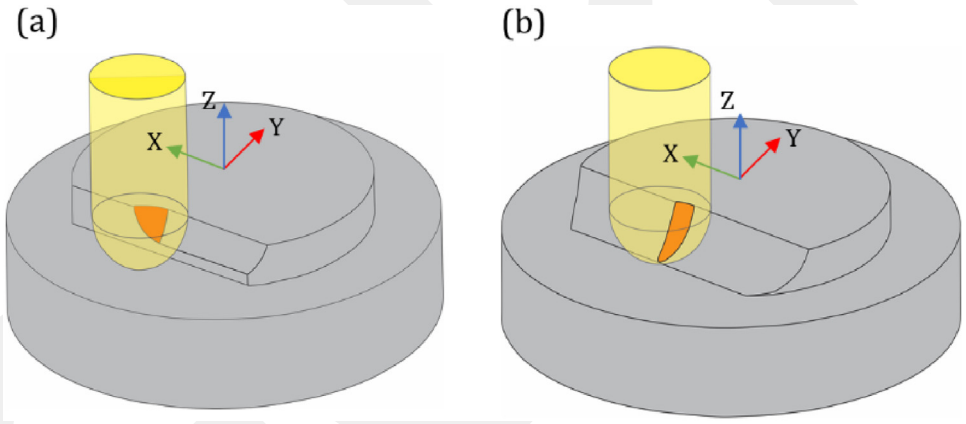

Fig. 10. Ball-end milling engagement area: (a) 4th pass, and (b) 6th pass down milling.

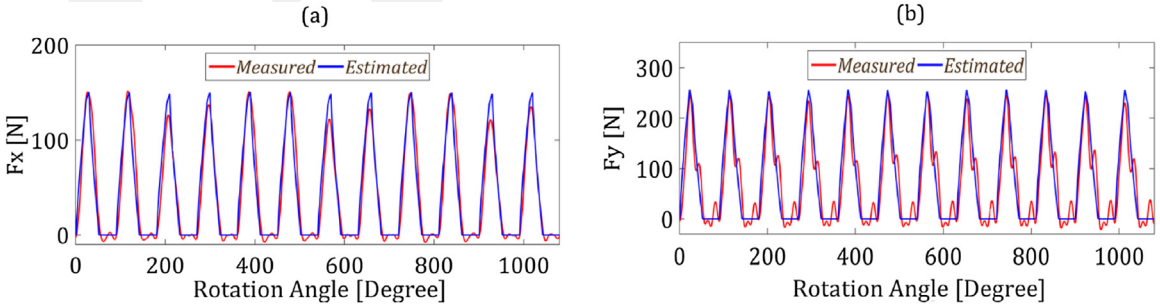

Fig. 11. Comparison between the measured and estimated cutting forces for 4th pass down-milling with the feedrate of 480 [mm/min]: Cutting forces in (a) the *X* direction, and (b) the *Y* direction.

optimal match can be attributed to the potential errors during the machining operation that caused the radial cutting forces to be lower than expected. Regardless, our estimation was successful in predicting the resultant forces (tangential and radial combine) with minimal errors.

Ball-end milling of 48-2-2 γ-TiAl

Down-end milling operations were performed using two different engagement conditions as shown in Fig. 10. A comparison between the simulation and the experimental data for these

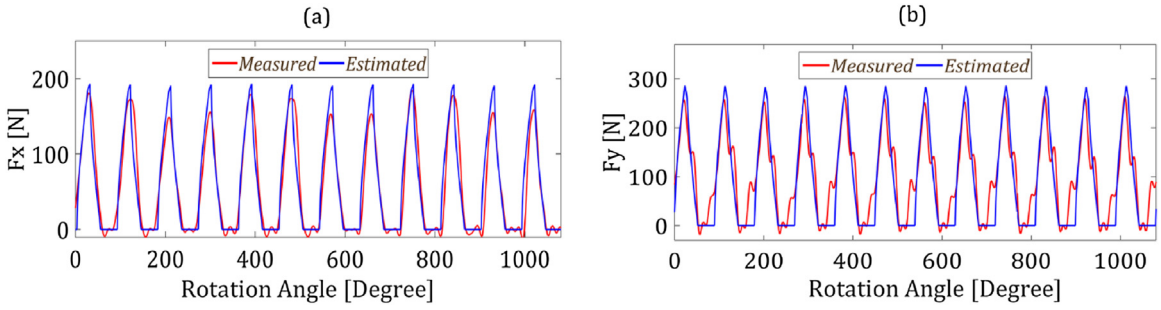

Fig. 12. Comparison between the measured and estimated cutting forces for 6th pass down-milling with the feedrate of 480 [mm/min]: Cutting forces in (a) the *X* direction, and (b) the *Y* direction.

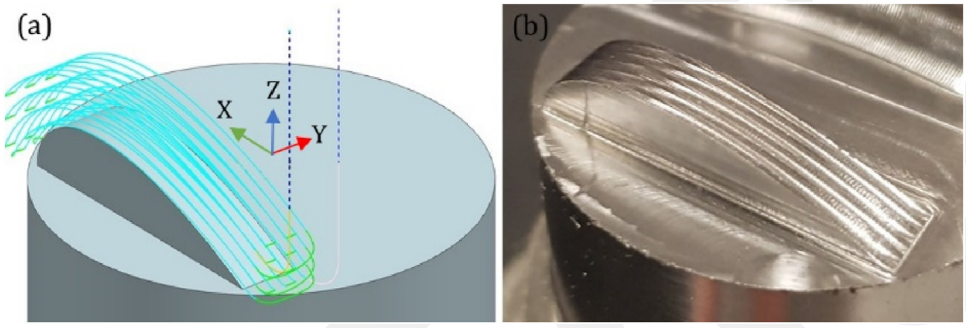

Fig. 13. (a) Cutting tool path for an airfoil geometry; (b) machined part.

engagement conditions are shown in Figs. 11 and 12; validation tests showed that the simulated and measured cutting forces match well within a 15% error band.

NACA 2429 airfoil profile was machined to validate the accuracyof orthogonal parameters for 48-2-2 γ-TiAl on freeform surfaces as shown in Fig. 13. The machining was performed in 4 layers with 6 paths in each layer. Estimated and measured cutting forces in the X and Y directions for the third path in the fourth layer are shown in Fig. 14. It can be inferred that the trend and the magnitude of the simulated and experimental cutting forces are in good agreement. The deviation in the cutting forces can be attributed to the instabilities that occur during machining operations.

Chip morphology of 48-2-2 γ-TiAl.

The chip morphology observation during the turning and milling operation confirmed a serrated, discontinuous and segmented chip geometry for all the cutting conditions. This phenomenon is due to the brittleness and low fracture toughness

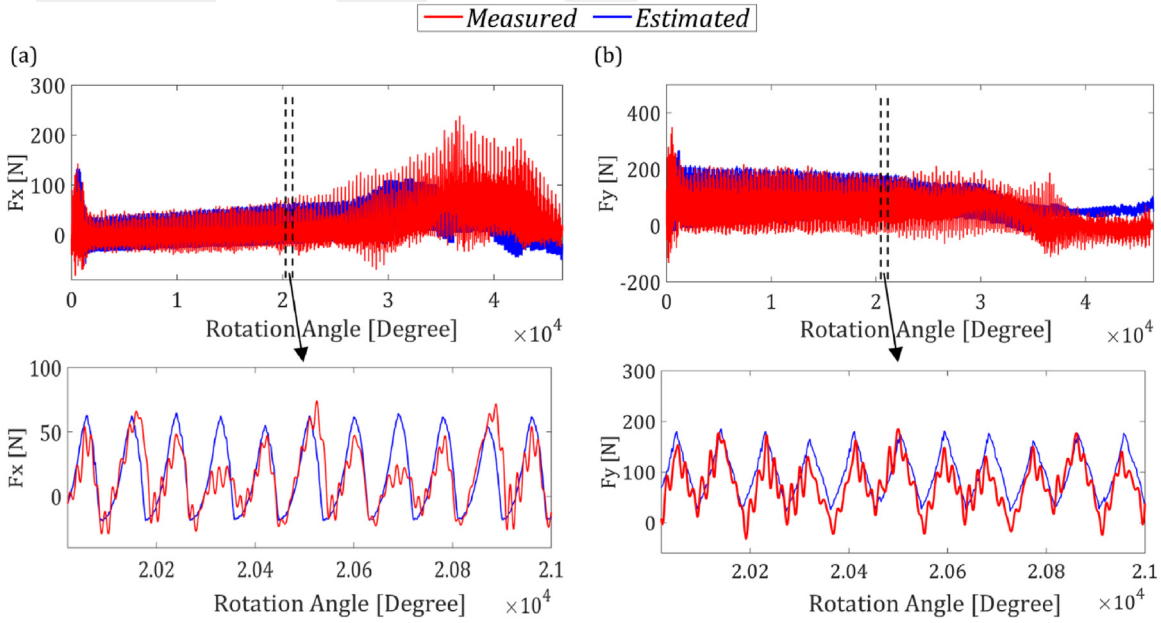

Fig. 14. Comparison between the measured and estimated cutting forces of the 4th layer, 3rd tool pass with 576 [mm/min] feedrate; close-up view for cutting forces in (a) the *X* direction and (b) the *Y* direction.

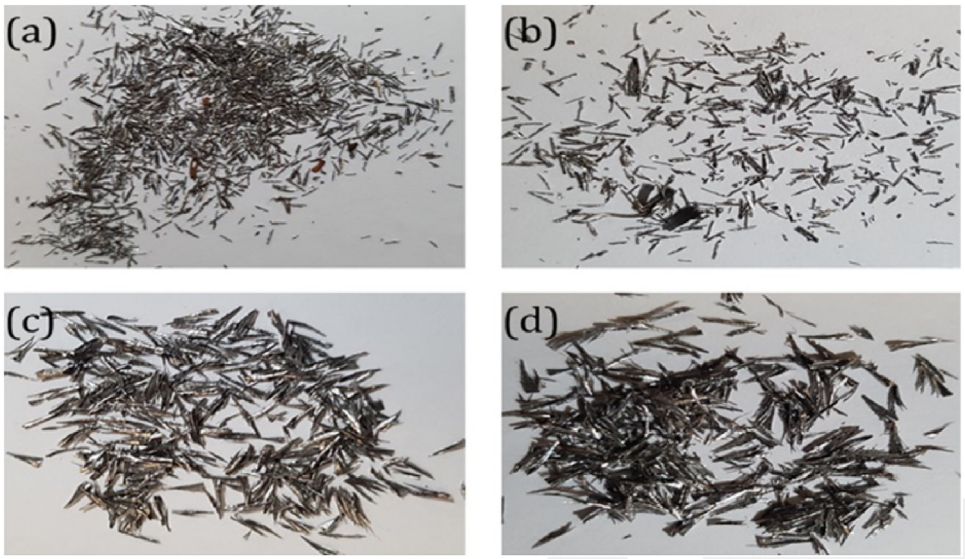

Fig. 15. Chip morphology of 48-2-2 γ-TiAl; in orthogonal turning at (a) 0.08 mm feedrate, (b) 0.100 mm feedrate, and in ball-end milling at (c) 336 mm/min feedrate, (d) 480 mm/min feedrate.

of γ-TiAl. Fig. 15 illustrates the chip morphology in the orthogonal turning and milling processes.

Conclusion

The article presents the formation of an orthogonal database to predict the fundamental cutting parameters of 48-2-2 γ-TiAl for the first time in literature. The effect of coating on friction coefficient, shear stress, shear angle and cutting forces are also investigated. The shear angle for AlCrN coated tool was found to be less than the AlTiN coated tool, and the friction coefficient for the AlCrN coated tool was observed to be greater than the AlTiN coated tool. The developed database is employed to predict the cutting forces of 48-2-2 γ-TiAl for milling operation. An analytical force model was used to simulate the cutting forces for end milling and ball-end milling for different coatings and cutting conditions. Estimated cutting forces, validated via end milling experiments, were found within 13% and 20% error band for AlCrN and AlTiN coatings, whereas cutting forces validated via ball-end milling experiments matched well within 15% error band for AlCrN coating. This study aims to be an important guide for machining of 48-2-2 γ-TiAl alloys and facilitating the transition from processing traditional materials to advanced materials for manufacturing industries.

Declaration of Competing Interest

The authors declare that they have no known competing financial interests or personal relationships that could have appeared to influence the work reported in this paper.

Acknowledgments

The authors would like to thank the Scientific Research Council of Turkey (TUBITAK Project No: 9140039), Basque Government (AeroTiAl, Project number: ZL-2017/000245) and H2020 (MMTech, project number: GA633776) for their financial support provided to the collaborative research project.

References

[1] Klocke, F., Lung, D., Arft, M., Priarone, P.C., Settineri, L., 2013, On high-speed turning of a third-generation gamma titanium aluminide. Int J Adv Manuf Technol, 65:155–163. http://dx.doi.org/10.1007/s00170-012-4157-5.

[2] Kothari, K., Radhakrishnan, R., Wereley, N.M., 2012, Advances in gamma titanium aluminides and their manufacturing techniques. Prog Aerosp Sci, 55:1–16. http://dx.doi.org/10.1016/j.paerosci.2012.04.001.

[3] Mantle, A.L., Aspinwall, D.K., 1997, Surface integrity and fatigue life of turned gamma titanium aluminide. J Mater Process Technol, 72:413–420. http://dx.doi.org/10.1016/S0924-0136(97)00204-5.

[4] Aspinwall, D.K., Dewes, R.C., Mantle, A.L., 2005, The machining of γ-TiAl intermetallic alloys. CIRP Ann, 54:99–104. http://dx.doi.org/10.1016/S0007-8506(07)60059-6.

[5] Hood, R., Cooper, P., Aspinwall, D.K., Soo, S.L., Lee, D.S., 2015, Creep feed grinding of γ-TiAl using single layer electroplated diamond superabrasive wheels. CIRP J Manuf Sci Technol, 11:36–44. http://dx.doi.org/10.1016/j.cirpj.2015.07.001.

[6] Mantle, A.L., Aspinwall, D.K., 2001, Surface integrity of a high speed milled gamma titanium aluminide. J Mater Process Technol, 118:143–150. http://dx.doi.org/10.1016/S0924-0136(01)00914-1.

[7] Priarone, P.C., Rizzuti, S., Settineri, L., Vergnano, G., 2012, Effects of cutting angle, edge preparation, and nano-structured coating on milling performance of a gamma titanium aluminide. J Mater Process Technol, 212:2619–2628. http://dx.doi.org/10.1016/j.jmatprotec.2012.07.021.

[8] Beranoagirre, A., Olvera, D., López De Lacalle, L.N., 2012, Milling of gamma titanium-aluminum alloys. Int J Adv Manuf Technol, 62:83–88. http://dx.doi.org/10.1007/s00170-011-3812-6.

[9] Settineri, L., Priarone, P.C., Arft, M., Lung, D., Stoyanov, T., 2014, An evaluative approach to correlate machinability, microstructures, and material properties of gamma titanium aluminides. CIRP Ann Manuf Technol, 63:57–60. http://dx.doi.org/10.1016/j.cirp.2014.03.068.

[10] Hood, R., Aspinwall, D.K., Soo, S.L., Mantle, A.L., Novovic, D., 2014, Workpiece surface integrity when slot milling γ-TiAl intermetallic alloy. CIRP Ann Manuf Technol, 63:53–56. http://dx.doi.org/10.1016/j.cirp.2014.03.071.

[11] Budak, E., Altintaş, Y., Armarego, E.J.A., 1996, Prediction of milling force coefficients from orthogonal cutting data. J Manuf Sci Eng, 118:216–224.

[12] Lazoglu, I., Boz, Y., Erdim, H., 2011, Five-axis milling mechanics for complex free form surfaces. CIRP Ann Manuf Technol, 60:117–120. http://dx.doi.org/10.1016/j.cirp.2011.03.090.

[13] Layegh, S.E., Lazoglu, K.I., 2017, 3D surface topography analysis in 5-axis ball-end milling. CIRP Ann Manuf Technol, 66:133–136. http://dx.doi.org/10.1016/j.cirp.2017.04.021.

[14] Bobzin, K., 2017, High-performance coatings for cutting tools. CIRP J Manuf Sci Technol, 18:1–9. http://dx.doi.org/10.1016/j.cirpj.2016.11.004.

[15] Swain, N., Venkatesh, V., Kumar, P., Srinivas, G., Ravishankar, S., Barshilia, H.C., 2017, An experimental investigation on the machining characteristics of Nimonic 75 using uncoated and TiAlN coated tungsten carbide micro-end mills. CIRP J Manuf Sci Technol, 16:34–42. http://dx.doi.org/10.1016/j.cirpj.2016.07.005.

[16] Chiang, S.-T., Tsai, C.-M., Lee, A.-C., 1995, Analysis of cutting forces in ball-end milling. J Mater Process Technol, 47:231–249. http://dx.doi.org/10.1016/0924-0136(95)85001-5.

[17] Gradišek, J., Kalveram, M., Weinert, K., 2004, Mechanistic identification of specific force coefficients for a general end mill. Int J Mach Tools Manuf, 44:401–414. http://dx.doi.org/10.1016/j.ijmachtools.2003.10.001.

[18] Layegh, S.E., Lazoglu, K.I., 2014, A new identification method of specific cutting coefficients for ball end milling. Proc CIRP, 14:182–187. http://dx.doi.org/10.1016/j.procir.2014.03.059.

[19] Yao, Z.Q., Liang, X.G., Luo, L., Hu, J., 2013, A chatter free calibration method for determining cutter runout and cutting force coefficients in ball-end milling. J Mater Process Technol, 213:1575–1587. http://dx.doi.org/10.1016/j.jmatprotec.2013.03.023.
[20] Zhang, X., Zhang, J., Zheng, X., Pang, B., Zhao, W., 2017, Tool orientation optimization of 5-axis ball-end milling based on an accurate cutter/workpiece engagement model. CIRP J Manuf Sci Technol, 19:106–116. http://dx.doi.org/10.1016/j.cirpj.2017.06.003.
[21] Altintas YY., (Ed.) (2012), Manufacturing automation, in: manufacturing automation: metal cutting mechanics, machine tool vibrations, and CNC design. 2nd ed. Cambridge University Press, Cambridge, pp. pp.xiii–xiv. http://dx.doi.org/10.1017/CBO9780511843723.002.
[22] Merchant, M.E., 1945, Mechanics of the metal cutting process. II. Plasticity conditions in orthogonal cutting. J Appl Phys, 16:318–324. http://dx.doi.org/10.1063/1.1707596.
[23] Yigit, I.E., SEL, K., Lazoglu, I., 2015, A solid modeler based engagement model for 5-axis ball end milling. Proc CIRP, 31:179–184. http://dx.doi.org/10.1016/j.procir.2015.03.051.
[24] Stanford, M., Lister, P.M., Morgan, C., Kibble, K.A., 2009, Investigation into the use of gaseous and liquid nitrogen as a cutting fluid when turning BS 970-80A15 (En32b) plain carbon steel using WC-Co uncoated tooling. J Mater Process Technol, 209:961–972. http://dx.doi.org/10.1016/j.jmatprotec.2008.03.003.
[25] Akmal, M., Layegh, K.S.E., Lazoglu, I., Akgün, A., Yavaş, Ç., 2017, Friction coefficients on surface finish of AlTiN coated tools in the milling of Ti6Al4V. Proc CIRP, 58:596–600. http://dx.doi.org/10.1016/j.procir.2017.03.231.
[26] Seifi, M., Ghamarian, I., Samimi, P., Ackelid, U., Collins, P., Lewandowski, J., 2016, Microstructure and mechanical properties of Ti-48Al-2Cr-2Nb manufactured via electron beam melting. Proc 13th world conf titan, 1317–1322. http://dx.doi.org/10.1002/9781119296126.ch223.
[27] Draper, S.L., Lerch, B.A., 2008, Durability assessment of TiAl alloys.. Retrieved from https://ntrs.nasa.gov/archive/nasa/casi.ntrs.nasa.gov/20080047349.pdf.